In vivo two-photon calcium imaging of neuronal networks

Christoph Stosiek*, Olga Garaschuk*, Knut Holthoff, and Arthur Konnerth†

Physiologisches Institut, Ludwig-Maximilians Universität München, Pettenkoferstrasse 12, 80336 Munich, Germany

Communicated by Clay M. Armstrong, University of Pennsylvania School of Medicine, Philadelphia, PA, April 16, 2003 (received for review January 31, 2003)

Two-photon calcium imaging is a powerful means for monitoring the activity of distinct neurons in brain tissue *in vivo*. In the mammalian brain, such imaging studies have been restricted largely to calcium recordings from neurons that were individually dye-loaded through microelectrodes. Previous attempts to use membrane-permeant forms of fluorometric calcium indicators to load populations of neurons have yielded satisfactory results only in cell cultures or in slices of immature brain tissue. Here we introduce a versatile approach for loading membrane-permeant fluorescent indicator dyes in large populations of cells. We established a pressure ejection-based local dye delivery protocol that can be used for a large spectrum of membrane-permeant indicator dyes, including calcium green-1 acetoxymethyl (AM) ester, Fura-2 AM, Fluo-4 AM, and Indo-1 AM. We applied this dye-loading protocol successfully in mouse brain tissue at any developmental stage from newborn to adult *in vivo* and *in vitro*. *In vivo* two-photon Ca^{2+} recordings, obtained by imaging through the intact skull, indicated that whisker deflection-evoked Ca^{2+} transients occur in a subset of layer 2/3 neurons of the barrel cortex. Thus, our results demonstrate the suitability of this technique for real-time analyses of intact neuronal circuits with the resolution of individual cells.

The question of how neuronal networks accomplish information processing is central for the understanding of higher brain functions. This question is difficult to answer, not only because of the immense number of computing elements, but also because of the difficulties of direct real-time monitoring of network activity. So far, the function of neuronal networks *in vivo* has been assessed mostly by extracellular multielectrode recordings (1) or by large-scale brain imaging techniques, including functional magnetic resonance imaging, positron-emission tomography, imaging of intrinsic optical signals, and voltage-sensitive dye-based imaging (2–6). A real-time analysis of neuronal networks *in vivo* is so far best achieved by using the powerful approach of voltage-sensitive dye-based imaging (4). Over the years these techniques have been used extensively for studying different aspects of brain function and have led to the discovery of important macroscopic features of processing networks, such as, for example, the orientation preference map in the visual cortex (7). However, many aspects of signal processing at the single-cell level as well as the temporal dynamics in processing neuronal networks have remained unclear.

Fluorometric Ca^{2+} imaging is another sensitive method for monitoring neuronal activity (8, 9). It makes use of the fact that in living cells, most depolarizing electrical signals are associated with Ca^{2+} influx attributable to the activation of one or more of the numerous types of voltage-gated Ca^{2+} channels, abundantly expressed in the nervous system (10, 11). These signals are often amplified further by Ca^{2+} release from intracellular Ca^{2+} stores (10, 11). Such Ca^{2+} signals are essential for elementary forms of neuronal communication, such as chemical synaptic transmission (12–15). In addition, Ca^{2+} signaling is obligatory for complex processes, such as the induction of memory- and learning-related forms of neuronal plasticity (16). Furthermore, many aspects of development at the beginning of a neuron's life, including gene expression, neuronal migration, and neurite outgrowth require transient intracellular elevations in Ca^{2+} concentration (17–20), whereas, paradoxically, Ca^{2+} transients are also involved in neuronal cell death (11).

The advantage of Ca^{2+} imaging is that it allows real-time analyses of individual cells and even subcellular compartments. At the same time it readily permits simultaneous recordings from many individual cells and has been used successfully in numerous *in vitro* studies in tissue cultures and brain slices. With the development of two-photon fluorescence microscopy, Ca^{2+} imaging *in vivo*, in neurons located up to 500 μm below the cortical surface, has become possible (21). In demanding experiments, Svoboda *et al.* (21, 22) measured Ca^{2+} transients in dendrites of neurons in the barrel cortex during spontaneous and evoked action potential firing as well as during sensory stimulation. A similar approach was used by Charpak *et al.* (23) for monitoring odor-evoked calcium signals in mitral cells of the rat olfactory bulb. So far, however, high-resolution Ca^{2+} imaging *in vivo* has been restricted mostly to a single neuron at any one time and, therefore, has not been used for monitoring neuronal networks directly. This limitation was imposed by the necessity of impaling a cell of interest with an intracellular electrode to load it with an indicator dye. *In vivo* Ca^{2+} imaging of populations of neurons has been attempted by using dextran-bound Ca^{2+} indicators (24). The study of Wachowiak *et al.* (25), who used calcium green dextran to monitor axonal Ca^{2+} signals in anterogradely labeled olfactory receptor neurons, is one of the few examples of such an imaging study in mammals *in vivo*. Although this approach is very useful for investigating synaptic inputs to olfactory bulb glomeruli, its spatial resolution relies entirely on the well-defined pattern of axonal connections in this system. For *in vitro* experiments there exists an alternative and simple method for loading cells with Ca^{2+} indicator dyes. For loading, slices or cell cultures are incubated in an external saline containing the membrane-permeant acetoxymethyl (AM) ester form of the dye (26). When combined with two-photon Ca^{2+} imaging, this staining technique allows simultaneous monitoring of the activity of thousands of individual neurons located up to 200 μm below the surface of a slice (27). Unfortunately, even *in vitro* the technique is often restricted to cells in culture or to slices of neonatal tissue (28).

The aim of the present study was to develop an approach that would allow the use of AM esters of Ca^{2+} indicators for staining populations of neurons *in vivo*, independent, if possible, of the age of the experimental animals.

Materials and Methods

***In Vivo* Loading of Cell Populations with Ca^{2+} Indicator Dyes.** Animal care was in accordance with institutional guidelines and was approved by the local government. BALB/c mice [1–17 days old (P1–17), $n = 23$] were anesthetized with either ketamine/xylazine or urethane (0.1/0.01 mg/g and 1.9 mg/g of body

Abbreviations: AM, acetoxymethyl; P*n*, postnatal day *n*; OG-1, Oregon green 488 BAPTA-1 [BAPTA is 1,2-bis(o-aminophenoxy)ethane-*N,N,N′,N′*-tetraacetic acid]; MCBL, multicell bolus loading.

*C.S. and O.G. contributed equally to this work.

†To whom correspondence should be addressed. E-mail: konnerth@lrz.uni-muenchen.de.

NEUROSCIENCE

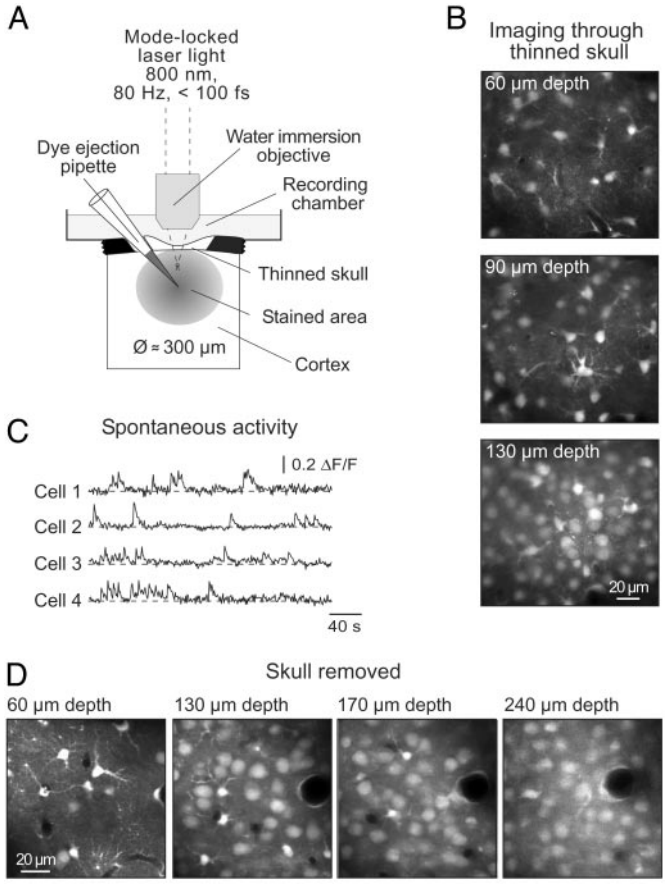

Fig. 1. *In vivo* calcium imaging of neuronal populations. (*A*) Schematic drawing of the experimental arrangement. (*B*) Images taken through a thinned skull of a P13 mouse at increasing depth. (*C*) Spontaneous Ca^{2+} transients recorded in a different experiment through a thinned skull in individual neurons (P5 mouse) located 70 μm below the cortical surface, from a region similar to that shown in *B*. (*D*) Images obtained as in *B* in an experiment (P13 mouse) in which the skull was removed before imaging.

weight, respectively, i.p.). Adult (4-month-old) mice were anesthetized by inhalation of isoflurane (1.5% in pure O_2). Depth of anesthesia was assessed by monitoring pinch withdrawal and eyelid reflex as well as respiration rate. The skull over the barrel cortex was thinned under a dissection microscope by using stainless still drill bits and polished with a felt polisher (Dr. Ihde Dental, Munich). The custom-made recording chamber with a hole in the middle was then glued to the skull with cyanoacryl glue (see Fig. 1*A*). The mouse was transferred into the set-up and placed onto a warming plate (38°C). The recording chamber was perfused with a warm (37°C) external saline containing, in mM: 125 NaCl, 2.5 KCl, 26 $NaHCO_3$, 1.25 NaH_2PO_4, 2 $CaCl_2$, 1 $MgCl_2$, 20 glucose, pH 7.4, when bubbled with 95% O_2/5% CO_2. A small craniotomy (≈1 mm) was performed above an area devoid of big blood vessels by using a thin (30 gauge) injection needle. AM ester of an indicator dye was dissolved in DMSO plus 20% Pluronic F-127 (e.g., 2 g of Pluronic F-127 in 10 ml of DMSO) to yield a concentration of 10 mM. For cell loading this solution was diluted 1/10 with a standard pipette solution containing, in mM: 150 NaCl, 2.5 KCl, 10 Hepes, pH 7.4, yielding a final dye concentration of 1 mM. A micropipette was filled with this solution and inserted coaxially into the cortex. A pressure pulse [1 min, 0.7 bar (1 bar = 100 kPa); Picospritzer II, General Valve, Fairfield, NJ] was applied to the pipette to eject ≈400 fl of the dye-containing solution. The volume of the ejected solution was estimated by injecting Fura-2 AM into an agar block (2% agarose, Sigma) and measuring the maximal diameter of the fluorescing sphere by means of two-photon microscopy. The same loading procedure was used in cortical slices.

For loading of calcium green-1 dextran (molecular weight 3,000 or 10,000) the dye was dissolved (12.5% solution) in the standard pipette solution and applied through micropipettes similar to those used for injections of AM indicator dyes, for various times (1–120 min) under the pressure of 0.7–1.4 bar.

Two-Photon Imaging. Imaging was performed by using a custom-built two-photon laser-scanning microscope based on a mode-locked laser system operating at 800 nm, 80-MHz pulse repeat, <100-fs pulse width (Tsunami and Millenia Xs, Spectra Physics, Mountain View, CA) and a laser-scanning system (Olympus Fluoview, Olympus, Tokyo) coupled to an upright microscope (BX51WI, Olympus) and equipped with one of the following water-immersion objectives: ×10, 0.3 numerical aperture (NA); ×20 0.95 NA; ×40, 0.8 NA; ×60, 0.9 NA; all from Olympus) or ×60 1.0 NA (Fluor ×60, Nikon, Tokyo). The average power delivered to the brain was <70 mW. Images were analyzed off-line with a LABVIEW-based custom-made software package (National Instruments, Austin, TX) and IGOR software (WaveMetrics, Lake Oswego, OR). Data are presented as the relative change in fluorescence ($\Delta F/F$).

Whisker Deflection and Electrical Stimulation *in Vivo*. For each trial the majority of whiskers on the contralateral side of the snout were deflected in caudal-to-rostral direction by a single 500-ms air puff (0.7 bar) applied through a thin glass capillary connected to a Picospritzer II. To avoid direct sensory stimulation of the skin, the capillary was positioned in a way that it blew away from the mouse's snout.

For electrical stimulation, voltage (30–70 V, 100–200 μs) pulses were passed through pipettes, similar to the ones used for injections of AM indicator dyes, filled with the external saline. The ground electrode was positioned in the recording chamber.

Electrophysiological Recordings and Drug Application. Coronal cortical slices (400 μm thick) were prepared from 18 BALB/c mice aged from P5 to P71, as previously described (27, 29). Membrane potentials were recorded with an EPC-9 patch-clamp amplifier (HEKA, Lambrecht, Germany) by using patch pipettes (resistance 4–5 MΩ) filled with an intracellular solution containing, in mM: 140 KCl, 10 NaCl, 4 MgATP, 0.4 NaGTP, 20 or 50 μM Oregon green 488 BAPTA-1 [OG-1; BAPTA is 1,2-bis(*o*-aminophenoxy)ethane-*N,N,N′,N′*-tetraacetic acid] hexapotassium salt, and 10 Hepes (pH 7.3, adjusted with KOH). For whole-cell patch-clamp experiments KCl and NaCl were replaced by 130 mM CsCl and 20 mM tetraethylammonium chloride. The series resistance was 12–16 MΩ.

Glutamate (10 mM) was applied by using an MVCS-C-01 iontophoresis system (ejection current −1 μA, duration 300–500 ms; NPI Electronic, Tamm, Germany) with a micropipette having a resistance of 10–12 MΩ when filled with a glutamate-containing external saline. A retaining current of +20 nA was imposed between applications to prevent leakage of glutamate.

Data are presented as mean ± SEM.

Results

Fig. 1*A* illustrates the basic approach used to stain large populations of neurons *in vivo* with Ca^{2+} indicator dyes (see also *Materials and Methods*). A pipette containing the AM ester form of an indicator dye was inserted into the cortex through an ≈1-mm-wide skull opening. The pipette was advanced along its axis until it reached the desired depth (usually 150–200 μm below the cortical surface), and ≈400 fl of the dye-containing solution was pressure-ejected (0.7 bar, 1 min). The pipette

resistance was 6–9 MΩ when filled with the loading solution (see *Materials and Methods* for composition) and was continuously monitored during the dye ejection. We tested various indicator dyes, including Fura-PE3 AM (Fig. 1*B*), Fura red AM, Indo-1 AM, calcium green-1 AM (Fig. 1*C*), OG-1 AM (Figs. 1*D*, 2, 3 *C–D*, 4, and 5), Fluo-4 AM, and magnesium green AM (Fig. 3 *A* and *B*). Despite earlier observations that, in slices, some Ca^{2+} indicators work better than others (28), all dyes seemed to be taken up by neurons equally well under our *in vivo* conditions. We termed this staining approach multicell bolus loading (MCBL).

The dye-loaded cells were visualized by using two-photon fluorescence microscopy (Fig. 1*A*; ref. 30). Because craniotomies are often accompanied by marked breath- and heartbeat-related movement artifacts (2, 31), we tried to image cells through the intact skull. We found that if the skull was thinned down to a thickness of 8–10 μm, individual cells could be well resolved up to 200 μm below the cortical surface (Fig. 1*B*). Removing the skull above the imaging field further improved depth resolution (Fig. 1*D*), allowing the detection of individual cells up to 300 μm below the cortical surface. It should be noted that the stability of recordings depended critically on the diameter of the craniotomy. Thus, openings larger than 1 mm in diameter were often accompanied by movement artifacts occurring at the heartbeat frequency. Cells stained with various indicator dyes were spontaneously active (see Fig. 1*C* for an example with calcium green-1 AM) and responded to electrical stimulation as well as to glutamate application with an increase in the intracellular Ca^{2+} concentration (see below).

To estimate the size of the stained area we removed the brains at the end of experiment and cut them in slices. First, we confirmed in 3/3 brains that the stained area was located within the barrel cortex. This conclusion was based on the slice anatomy and on the fact that by using bright-field optics barrel-like structures were seen clearly in layer 4. We then measured the diameter of the stained area both in the *in vivo* stained and sliced brains and, separately, in the intact *in vivo* imaged brains. In both cases, dye injections 150–200 μm below the cortical surface resulted in almost spherical stained areas (Fig. 2*A*) covering cortical layers 1–3. The median diameter of the stained regions was ≈300 μm (Fig. 2*B*, left column; $n = 13$ mice), although the diameters of the stained areas in sliced brains (red circles in Fig. 2*B*) appeared to be slightly larger than those *in vivo* (red squares in Fig. 2*B*). This difference is probably due to the dim cells at the edge of the stained area emitting too little fluorescence to be detected *in vivo*. Of note, MCBL was readily applicable to acutely prepared cortical slices (see below), yielding stained areas of comparable dimensions (Fig. 2*B*, right column).

As shown in Fig. 2 *C* and *D*, a stable level of fluorescence within stained cells was reached ≈1 h after dye ejection. There was no major difference in the time course of dye loading *in vivo* ($n = 7$) and *in vitro* ($n = 9$). At intensities of the excitation light used to image stained cells virtually no autofluorescence of the cortical tissue was detected either *in vitro* (tissue next to the stained area in Figs. 2*A* and 3*A*) or *in vivo* (not shown). With time, fluorescence intensity decreased in stained cells, most likely reflecting the leakage of the dye. The leakage rate was estimated *in vitro* by measuring mean fluorescence levels at 5-min intervals for 6 h, starting 1 h after the dye ejection ($n = 3$, Fig. 2*D*). Despite the fact that the stained slices were kept at 34–37°C, the leakage rate was relatively low, resulting in less than 25% loss of peak fluorescence intensity in 6 h. *In vivo* it was possible to conduct continuous experiments for 4–6 h without any significant dye leakage and/or bleaching. The longest recording session conducted first *in vivo* and then *in vitro* lasted for 10 h. Thus, our loading technique provides stable staining conditions for neurons both *in vivo* and *in vitro* with apparently better results *in vivo*.

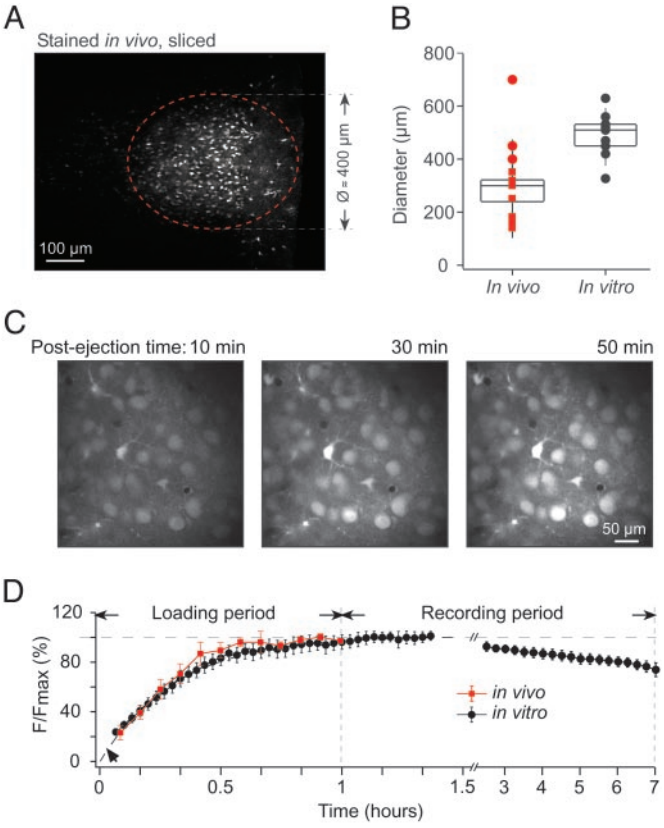

Fig. 2. Effectiveness and time-course of the staining procedure. (*A*) Image of the stained area in a cortical slice obtained from a P13 mouse (×20 objective). The cells were stained *in vivo*, and the brain was then removed and sliced. (*B*) Box plot of data illustrating the diameter of the stained area in different experiments. Each symbol marks a separate experiment. Squares ($n = 10$) represent cortices stained and imaged *in vivo*, and circles represent cortices imaged *in vitro* and stained either *in vivo* ($n = 3$, red symbols) or *in vitro* ($n = 10$, black symbols). (*C*) Consecutive images taken *in vivo* at 90-μm depth 10, 30, and 50 min after ejection (1 min) of 1 mM OG-1 AM into the cortex of a P14 mouse. (*D*) Normalized mean fluorescence intensity as a function of postejection time. The plot summarizes data obtained in seven *in vivo* (red squares) and nine *in vitro* (black circles) experiments (left part of the graph) and in three *in vitro* (black circles) experiments (right part of the graph).

Previously, we and others (see, for example, ref. 28) have experienced difficulties in loading neurons in brain slices from adult rodents with bath-applied AM indicator dyes. In contrast, MCBL provided excellent results in slices of adult mice (Fig. 3*A*). Surprisingly, the quality of staining appeared to be better in adults than in neonates. Not only all cell somata were detectable in adults, but also many cellular processes could be visualized (arrows in Fig. 3*A Right*). The healthy appearance of stained cells as well as their robust responses to iontophoretic glutamate applications (Fig. 3*B*) indicated the viability of our approach. Similar data were obtained in slices cut from *in vivo* stained adult brains ($n = 4$, not shown). Thus, MCBL is applicable for virtually noninvasive, in-depth staining of neurons in the adult brain.

To estimate the intracellular indicator dye concentration when using MCBL, the cells in cortical slices were first stained with OG-1 AM. Thereafter, one of the cells was patched and dialyzed with an intracellular solution containing either 20 or 50 μM OG-1 hexapotassium salt. The steady-state fluorescence intensity of the patched cell was used to estimate the dye concentration in the neighboring AM-loaded neurons. As shown in Fig. 3 *C* and *D*, on average, the dye concentration within intact neurons was close to 20 μM ($n = 35$ cells). We noticed, however, that cells

NEUROSCIENCE

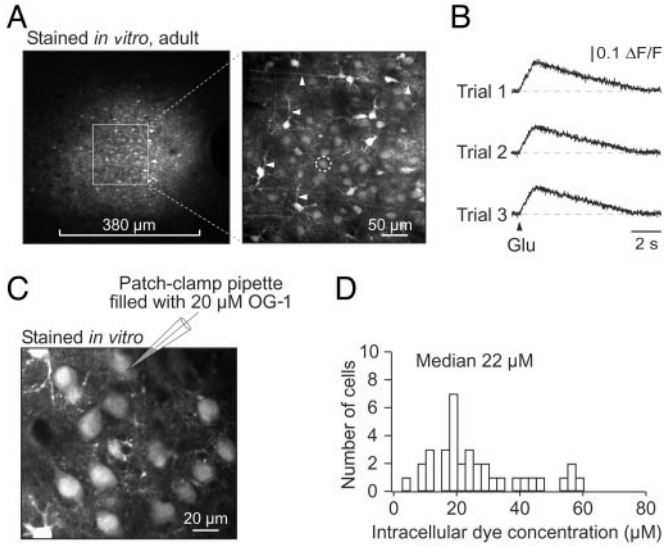

Fig. 3. *In vitro* staining of the adult mouse cortex. (*A Left*) An overview (taken with a ×20 objective) of the area in a cortical slice from a P71 mouse stained with magnesium green AM. (*Right*) A maximal projection of 10 images taken with a ×60 objective from 50 to 60 µm underneath the slice surface. The imaged area is delimited by the square area indicated in *Left*. (*B*) Line-scan recordings of Ca^{2+} transients in a neuron (marked with a white circle in *A Right*), evoked by three consecutive 350-ms iontophoretic glutamate applications. (*C*) Layer 2/3 cells in a cortical slice stained *in vitro* with OG-1 AM. After staining, one cell was patched and perfused with an intracellular solution containing 20 µM OG-1 hexapotassium salt. (*D*) Histogram illustrating the distribution of the estimated OG-1 concentration in neurons stained by using the MCBL technique.

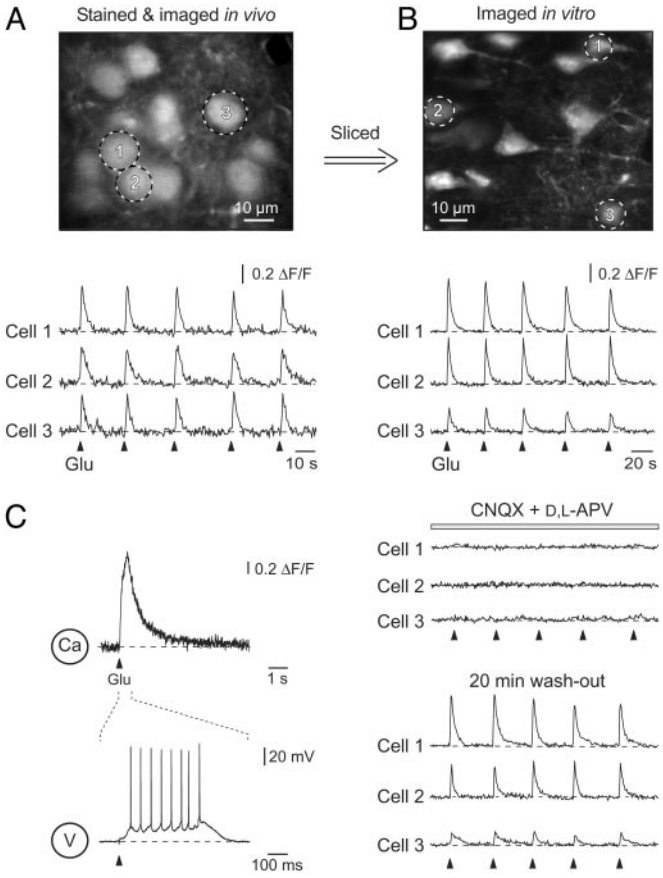

Fig. 4. *In vivo* and *in vitro* comparison of glutamate-evoked Ca^{2+} transients. (*A Upper*) A high-magnification image of layer 2/3 neurons *in vivo* in the cortex of a P13 mouse. (*Lower*) Ca^{2+} transients in three individual neurons (marked in *Upper*) evoked by five consecutive 500-ms iontophoretic glutamate applications. (*B Upper*) *In vivo* stained layer 2/3 neurons from the same mouse as in *A* visualized *in vitro* in a cortical slice. (*Lower*) Ca^{2+} transients in three individual neurons evoked by iontophoretic glutamate applications in control, in the presence of 10 µM 6-cyano-7-nitroquinoxaline-2,3-dione (CNQX) and 50 µM DL-2-amino-5-phosphonovaleric acid (APV), and 20 min after wash-out of the drugs. (*C*) Line-scan Ca^{2+} measurements and simultaneous recordings of membrane potential changes evoked by a 500-ms iontophoretic glutamate application in a whole-cell patch-clamped layer 2/3 pyramidal neuron.

with a glia-like appearance were always much brighter. The dye concentration in this type of cells reached levels of 80–100 µM ($n = 4$). Similar levels of cellular fluorescence in neuron- and glia-like cells were also obtained in slices from other brain regions, including hippocampus, thalamus, and cerebellum. It is important to note that MCBL did not cause any relevant dye compartmentalization in organelles, as often encountered with AM-dye loading protocols involving prolonged incubations. This finding was verified by staining cells in slices first with OG-1 AM and then patching them with dye-free pipette solutions. The resulting dialysis decreased the cell's fluorescence to nearly background levels (13.6 ± 3%, $n = 4$ cells). No "hot spots," indicative for dye molecules captured within organelles, were detected in high-resolution images of thereby unloaded cells.

To test the viability of stained neurons further, we stimulated layer 2/3 neurons *in vivo* by iontophoretic glutamate application (Fig. 4*A*). This stimulation resulted in transient increases in the intracellular calcium concentration in cells located in the vicinity (≤50 µm) of the application pipette (Fig. 4*A Lower*). The Ca^{2+} transients were caused by glutamate itself and not by the ejection current, because the same stimuli applied from a pipette containing no glutamate failed to induce any Ca^{2+} transients (data not shown). We next compared Ca^{2+} transients recorded *in vivo* with glutamate-activated Ca^{2+} transients obtained in layer 2/3 neurons in slices of the same *in vivo* stained brains. After slicing the brain, the neurons were stimulated by iontophoretic glutamate pulses similar to those used *in vivo* (Fig. 4*B*). These stimulations resulted in similar Ca^{2+} transients, which were reversibly blocked by a mixture of the α-amino-3-hydroxy-5-methyl-4-isoxazolepropionic acid (AMPA) and *N*-methyl-D-aspartate (NMDA) receptor antagonists 6-cyano-7-nitroquinoxaline-2,3-dione (CNQX) and 2-amino-5-phosphonovaleric acid (APV). As illustrated in Fig. 4*C*, in a whole-cell patch-clamped neuron such iontophoretic glutamate applications caused 520- to 590-ms trains of 8–12 action potentials ($n = 3$ cells).

Fig. 5 demonstrates that MCBL is suitable for monitoring somatic Ca^{2+} transients evoked in individual layer 2/3 neurons of the barrel cortex by whisker deflection. By using the line-scan mode (5 ms per line) we recorded whisker deflection-evoked Ca^{2+} transients (mean amplitude of 0.38 ± 0.07, $n = 9$ cells). The decay time constant of the transients was 140–390 ms and was comparable to the decay time constant of transients evoked by single-shock electrical stimulation (Fig. 5 *Inset*). To obtain an insight into how neighboring layer 2/3 neurons respond to the same sensory stimulus, groups of three cells were monitored simultaneously. We selected cells located along a straight line with at least one cell responding more than once during the first three stimuli. In 34% of the trials (total of 38 trials, three mice) all cells responded to the stimulus, in 36% of cases only a subset of cells responded, and in 30% of the trials, whisker deflection failed to produce Ca^{2+} responses in these three cells. At least one Ca^{2+} transient was recorded in each

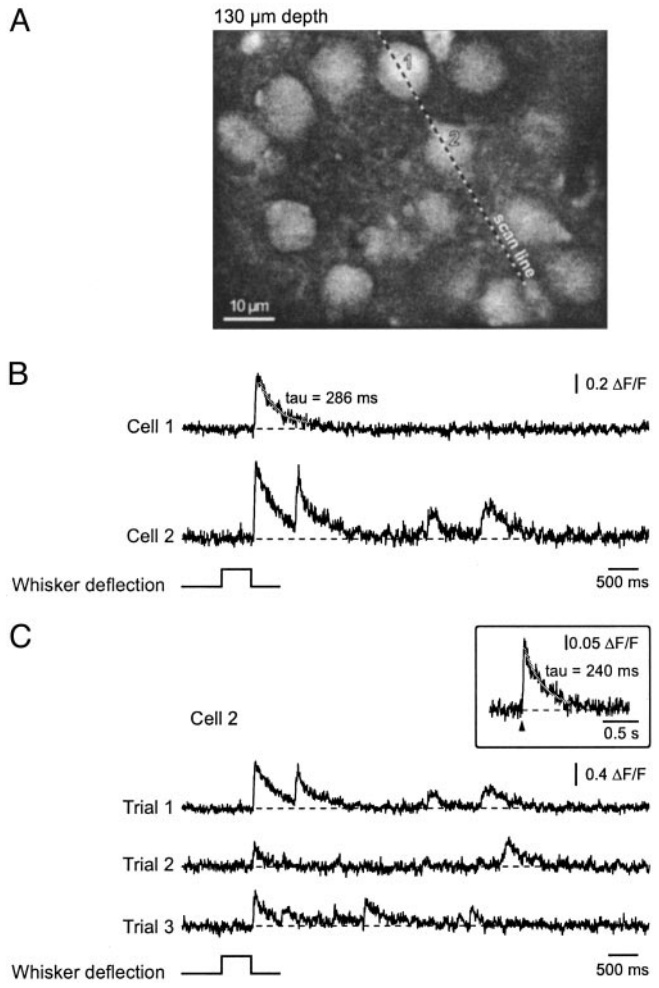

Fig. 5. *In vivo* recordings of Ca^{2+} transients evoked by whisker deflection. (*A*) A high-magnification image of layer 2/3 neurons *in vivo* in the barrel cortex of a P13 mouse. (*B*) Line-scan recordings of Ca^{2+} transients evoked in two neurons by a deflection of the majority of whiskers on the contralateral side of the mouse's snout. The position of the scanned line and the cells analyzed are indicated in *A*. Note that the Ca^{2+} transients occurred 17–22 ms after the termination of the stimulus and therefore probably represent stimulus-offset responses (42). Here and in *C*, the solid line represents a mono-exponential fit of the decay phase of the transient. (*C*) Ca^{2+} transients evoked in cell 2 during three consecutive trials. The top trace is from the trial illustrated in *B*. (*Inset*) A Ca^{2+} transient in a P14 layer 2/3 neuron evoked *in vivo* by single-shock electrical stimulation (70 V, 200 μs, average of five consecutive trials).

studied cell and the pattern of responding cells changed from trial to trial. Thus, in more than one-third of the trials, whisker deflections activated only a subset of neurons, indicating that even the global activation of all whiskers result in a mosaic activation pattern in the cortical layer 2/3.

Discussion

The approach introduced here permits simultaneous Ca^{2+} recordings in tens to hundreds of individual neurons. Importantly, it requires only minor surgery and allows, at least in young mice, neurons to be imaged through the intact, although thinned, skull. Leaving the skull intact not only helps to eliminate movement artifacts but also opens the possibility of long-lasting, perhaps even chronic, recordings (32) with the possibility of restaining the neurons if necessary. In addition, the MCBL technique provides a straightforward means for in-depth staining of neurons in the adult brain. If combined with a miniature head-mounted two-photon microscope (33), it may also allow *in vivo* two-photon imaging in freely moving animals.

The major difference between MCBL and other staining methods using AM indicator dyes is that in our study the indicators were delivered for a short period directly to the target cells. In particular, this approach improved the staining of neurons in the adult brain, which are, in general, not stained by bath-applied AM indicator dyes. Local dye delivery also allowed the size of the stained region to be controlled, thus permitting selective staining of areas of interest. Furthermore, MCBL is suitable for staining virtually any cell type, including all kinds of cortical, hippocampal, thalamic, and cerebellar neurons. Remarkably, it allows staining of cerebellar Purkinje cells, which are difficult to load with bath-applied AM indicator dyes at any developmental stage (ref. 34; unpublished observations). Our results suggest that MCBL can be used for loading cells *in vivo* and *in vitro* with any indicator dyes, including voltage-sensitive dyes, Na^+ and Cl^- indicators, lipophilic dyes such as DiO (3,3′-dioctadecyloxacarbocyaninine) and DiI (1,1′-dioctadecyl-3,3,3′,3′-tetramethylindocarbocyanine), etc. Last, but not least, MCBL needs only ≈400 fl of the dye-containing solution per experiment compared with the much larger quantities used for bath loading and is, therefore, also economically attractive.

In comparison to *in vivo* imaging of microelectrode-loaded cells, MCBL has, however, some obvious limitations. First, the depth limit in our recordings was ≈200 μm with and 300 μm without the skull, compared with 500 μm when imaging cell dendrites of microelectrode-loaded cells (21). This difference is partially due to the higher dye concentration in cells reached by microelectrode-loading procedures. Thus, MCBL-loaded cells contained up to 60 μM, on average 20 μM, indicator dye, instead of <3–6 mM when stained by using a microelectrode. Another problem is a reduced image contrast because of the staining of many fine processes in the surrounding neuropil. These two limitations make the use of MCBL for *in vivo* imaging of neuronal dendrites at present difficult. Future strategies for improving the quality of recordings include the use of longer wavelengths of the excitation light, larger numerical apertures of the objective lens, better transmittance of all lenses, beam splitters and filters, higher photon sensitivity of the photomultiplier tube, etc. Because the proportion of scattered photons in the emitted fluorescence signal increases markedly with increasing imaging depth, a larger craniotomy and a larger effective angular acceptance of the detection optics (35) should also significantly improve depth resolution by enabling the collection of larger portion of scattered photons. Finally, better results will be obtained with dyes having a larger two-photon cross section (30).

To date, the commonly used method for *in vivo* staining of neuronal populations with calcium indicator dyes has been to label them with dextran conjugates of the dyes (24, 36). This technique employs retrograde or anterograde transport of the dye and, thus, selectively stains neurons projecting to, or axonal fibers originating from, the site of dye application. The dextran-based staining procedure has been used *in vivo* to image population activity of spinal neurons in the zebra fish (37), to monitor light-induced Ca^{2+} transients in individual retinal axons of *Xenopus* tadpoles (38), and to record odor-induced Ca^{2+} signals in the olfactory bulb glomeruli of mouse and zebra fish (25, 39). Furthermore, by using a similar approach, Mulligan *et al.* (40) imaged individual neurons with a good signal-to-noise ratio near the injection site within the frog accessory olfactory bulb. Although both MCBL and the dextran-based staining technique are suited for *in vivo* staining of neurons, these approaches cannot substitute for each other. Whereas MCBL provides neuronal staining "here and now," the dextran-based staining technique requires prolonged time periods for dye uptake. We want to stress that we failed to label cells with dextran-

conjugated dyes when using the "mild" delivery protocol used for AM indicators (see *Materials and Methods* for details). We did not try, however, to improve dye uptake by using the usual cell-damaging procedures, such as adding the detergent Triton X-100 to the staining solution (24, 25, 39) or perforating cells with large dye-ejection pipettes [40- to 50-μm tip openings (36)]. Thus, under our conditions the dextran-conjugated dyes just accumulated in the extracellular space near the ejection site and were not taken up by neurons.

To test the usefulness of MCBL *in vivo*, we monitored Ca^{2+} transients in layer 2/3 neurons of the barrel cortex. Ca^{2+} transients, similar to those recorded in slices, were observed in response to either iontophoretic glutamate application or single-shock electrical stimulation. Importantly, we detected Ca^{2+} transients in clusters of neurons in response to whisker stimulation. These Ca^{2+} transients were caused most probably by one or two action potentials (21, 22, 41). The signal-to-noise ratio was sufficient to allow individual, nonaveraged somatic Ca^{2+} transients to be distinguished clearly from the background noise. The occurrence of these large Ca^{2+} transients in layer 2/3 neurons is surprising in view of the findings of Brecht and Sakmann (42), who performed *in vivo* patch-clamp recordings of individual layer 4 neurons in rats and found that these cells, which relay thalamic output to layer 2/3, exhibit very little whisker deflection-correlated action potential firing. On the other hand, Stern *et al.* (41) reported that whisker deflections often produce action potentials in layer 2/3 neurons of rats older than P20. In our recordings presumed action potential-generated Ca^{2+} transients were observed in mouse neurons already at P13. Our data suggest that on the level of individual layer 2/3 neurons, deflections of the majority of whiskers result in a mosaic activation pattern, which changes from trial to trial. This original finding is difficult to obtain with other approaches.

Our method provides a surprisingly simple and robust approach for imaging Ca^{2+} in cortical networks with single-cell resolution *in vivo*. We trust that this method will allow rapid progress in our understanding of neuronal interactions in the intact brain and, particularly, a better understanding of functional changes on the level of single neurons *and* networks in various mouse mutants.

We thank Y. Kovalchuk, W. K. Kafitz, and H. Adelsberger for valuable technical suggestions; J. Davis for comments on the manuscript; and R. Maul, S. Schickle, and I. Schneider for technical assistance. This work was supported by grants from the Deutsche Forschungsgemeinschaft (SFB 391 to O.G. and A.K.) and Graduiertenkolleg 333.

1. Nicolelis, M. & Ribeiro, S. (2002) *Curr. Opin. Neurobiol.* **12,** 602–606.
2. Shoham, D., Glaser, D. E., Arieli, A., Kenet, T., Wijnbergen, C., Toledo, Y., Hildesheim, R. & Grinvald, A. (1999) *Neuron* **24,** 791–802.
3. Raichle, M. E. (1998) *Proc. Natl. Acad. Sci. USA* **95,** 765–772.
4. Orbach, H. S., Cohen, L. B. & Grinvald, A. (1985) *J. Neurosci.* **5,** 1886–1895.
5. Grinvald, A., Frostig, R. D., Lieke, E. & Hildesheim, R. (1988) *Physiol. Rev.* **68,** 1285–1366.
6. Logothetis, N., Merkle, H., Augath, M., Trinath, T. & Ugurbil, K. (2002) *Neuron* **35,** 227–242.
7. Bonhoeffer, T. & Grinvald, A. (1991) *Nature* **353,** 429–431.
8. Tsien, R. Y. (1988) *Trends Neurosci.* **11,** 419–424.
9. Mao, B. Q., Hamzei-Sichani, F., Aronov, D., Froemke, R. C. & Yuste, R. (2001) *Neuron* **32,** 883–898.
10. Tsien, R. W. & Tsien, R. Y. (1990) *Annu. Rev. Cell Biol.* **6,** 715–760.
11. Berridge, M. J., Lipp, P. & Bootman, M. D. (2000) *Nat. Rev. Mol. Cell Biol.* **1,** 11–21.
12. Neher, E. (1998) *Neuron* **20,** 389–399.
13. Südhof, T. (2000) *Neuron* **28,** 317–320.
14. Yuste, R. & Denk, W. (1995) *Nature* **375,** 682–684.
15. Kovalchuk, Y., Eilers, J., Lisman, J. & Konnerth, A. (2000) *J. Neurosci.* **20,** 1791–1799.
16. Chittajallu, R., Alford, S. & Collingridge, G. L. (1998) *Cell Calcium* **24,** 377–385.
17. Buonanno, A. & Fields, R. D. (1999) *Curr. Opin. Neurobiol.* **9,** 110–120.
18. Gomez, T. M. & Spitzer, N. C. (1999) *Nature* **397,** 350–355.
19. Spitzer, N. C., Lautermilch, N. J., Smith, R. D. & Gomez, T. M. (2000) *BioEssays* **22,** 811–817.
20. Komuro, H. & Rakic, P. (1998) *J. Neurobiol.* **37,** 110–130.
21. Svoboda, K., Denk, W., Kleinfeld, D. & Tank, D. W. (1997) *Nature* **385,** 161–165.
22. Svoboda, K., Helmchen, F., Denk, W. & Tank, D. W. (1999) *Nat. Neurosci.* **2,** 65–73.
23. Charpak, S., Mertz, J., Beaurepaire, E., Moreaux, L. & Delaney, K. (2001) *Proc. Natl. Acad. Sci. USA* **98,** 1230–1234.
24. O'Donovan, M. J., Ho, S., Sholomenko, G. & Yee, W. (1993) *J. Neurosci. Methods* **46,** 91–106.
25. Wachowiak, M. & Cohen, L. B. (2001) *Neuron* **32,** 723–735.
26. Tsien, R. Y. (1981) *Nature* **290,** 527–528.
27. Garaschuk, O., Linn, J., Eilers, J. & Konnerth, A. (2000) *Nat. Neurosci.* **3,** 452–459.
28. Yuste, R. (2000) in *Imaging: A Laboratory Manual*, eds. Yuste, R., Lanni, F. & Konnerth, A. (Cold Spring Harbor Lab. Press, Plainview, NY), pp. 34.1–34.9.
29. Edwards, F., Konnerth, A., Sakmann, B. & Takahashi, T. (1989) *Pflügers Arch.* **414,** 600–612.
30. Denk, W., Strickler, J. H. & Webb, W. W. (1990) *Science* **248,** 73–76.
31. Margrie, T. W., Brecht, M. & Sakmann, B. (2002) *Pflügers Arch.* **444,** 491–498.
32. Christie, R. H., Bacskai, B. J., Zipfel, W. R., Williams, R. M., Kajdasz, S. T., Webb, W. W. & Hyman, B. T. (2001) *J. Neurosci.* **21,** 858–864.
33. Helmchen, F., Fee, M. S., Tank, D. W. & Denk, W. (2001) *Neuron* **31,** 903–912.
34. Kirischuk, S. & Verkhratsky, A. (1996) *Pflügers Arch.* **431,** 977–983.
35. Oheim, M., Beaurepaire, E., Chaigneau, E., Mertz, J. & Charpak, S. (2001) *J. Neurosci. Methods* **111,** 29–37.
36. Kreitzer, A. C., Gee, K. R., Archer, E. A. & Regehr, W. G. (2000) *Neuron* **27,** 25–32.
37. Fetcho, J. R. & O'Malley, D. M. (1995) *J. Neurophysiol.* **73,** 399–406.
38. Edwards, J. A. & Cline, H. T. (1999) *J. Neurophysiol.* **81,** 895–907.
39. Friedrich, R. W. & Korsching, S. I. (1997) *Neuron* **18,** 737–752.
40. Mulligan, S. J., Davison, I. & Delaney, K. R. (2001) *Neuroscience* **104,** 137–151.
41. Stern, E., Maravall, M. & Svoboda, K. (2001) *Neuron* **31,** 305–315.
42. Brecht, M. & Sakmann, B. (2002) *J. Physiol.* **543,** 49–70.